Magnetic Structure of Chiral Graphene Nanoribbons

A thesis

by

James Kevin Pierce

BS, West Virginia University, 2013

A THESIS SUBMITTED IN PARTIAL FULFILLMENT OF
THE REQUIREMENTS FOR THE DEGREE OF

MASTER OF SCIENCE

in

The Faculty of Graduate and Postdoctoral Studies

(Physics)

THE UNIVERSITY OF BRITISH COLUMBIA

(Vancouver)

April 15 2016

Abstract

We study the magnetic structure of narrow graphene ribbons with patterned edges. Neglecting interactions, a broad class of edge terminations support zero-energy states localized at the edges of the ribbon. For the simplest (zigzag) ribbon supporting these edge states, electron-electron interactions have been shown to induce ferromagnetic ordering along the edges of the ribbon. We generalize this argument for such a magnetic edge state to carbon ribbons with more complex chiral edge terminations.

Preface

This thesis is original work by the author Kevin Pierce, created in collaboration with research supervisor Dr. Ian Affleck.

Table of Contents

List of Figures

Chapter 1

Introduction

Among its many allotropes, carbon forms one atom thick two-dimensional honeycomb ribbons with a wide variety of edge geometries [4]. The edge geometry of these ribbons is intimately connected to their electronic and magnetic properties, and for many of the simplest possible ribbon edges, it has been shown that electrons with energies exponentially small in the width of the ribbon will localize near the ribbon edge [1] [2]. Signatures of magnetic ordering among these zero-energy zigzag edge-localized electrons has been seen experimentally [5], and it has been rigorously proven that zigzag graphene ribbons will be ferromagnetic at their edges with an edge-projected Hubbard model in the limit $U/t \ll 1$ [8].

The topic of this thesis is a generalization of this rigorous proof of ferromagnetism in zigzag ribbons to a wider class of edge geometries called chiral ribbons. In chapter 2 we define the zigzag, armchair, and chiral geometries. In chapter 3 we will review the electronic and magnetic structure of zigzag ribbons, and in chapter 4 we will discuss the electronic structure of chiral ribbons in the absense of electron-electron interactions before we include electron-electron interactions to lowest order by projecting a Hubbard interaction onto the localized edge states of the non-interacting spectrum. This process will indicate a ferromagnetic ordering of localized edge electrons in several particular chiral graphene ribbons.

Graphene owes its hexagonal structure to the sp^2 hybridization of its carbon atoms. On each atom, the two p-orbitals oriented in the plane of the graphene sheet mix with the s orbital

One s-orbital and two p-orbitals hybridize in the plane of the graphene sheet, leading to a trigonal-planar structure bound by σ-bonds in the plane between neighbouring carbon atoms. The third p-orbital is oriented per-

pendicular to the plane and forms covalent π-bonds with its neighbours, generating a π-band. This π-band is half-filled since each π-orbital has one electron.

Such a half-filled band has strong tight-binding character, justifying the use of a local approximation. Graphene exhibits a large intra-site Coulomb interaction, with $U/t \approx 3.5$ in such a local approximation [15]. Graphene is a strongly interacting material. Nevertheless, we hope to glean information about its electronic and magnetic properties by projecting the interacting problem onto the non-interacting eigenstates in a small U/t limit. Within this approach we will show certain minimal chiral graphene ribbons have ferromagnetic ordering of electrons in their localized edge states.

Chapter 2

Geometry and Properties of Graphene Ribbons

The electronic structure of graphene ribbons is highly dependent on edge geometry. In this chapter we will discuss the geometry of graphene and define the zigzag, armchair, and minimal chiral edge terminations of graphene ribbons. The chapter will conclude with summaries of the electric and magnetic properties of these different edge geometries.

Graphene is a two-dimensional hexagonal arrangement of carbon atoms. A honeycomb lattice is not a Bravais lattice, but can be constructed from a triangular Bravais lattice with a basis of two atoms per unit cell. This triangular lattice is represented by two vectors as indicated in figure 2.1 which we represent as $\mathbf{R}_1 = (a, 0)$, $\mathbf{R}_2 = (a/2, \sqrt{3}a/2)$, where $a \approx 2.46$Å is the triangular lattice constant.

When the graphene sheet is terminated to form a ribbon, there are many possible edge geometries. The two simplest edge geometries are called zigzag and armchair. The next level of complication one can imagine for the edge terminations are the so-called minimal chiral ribbons, which are the concentration of the rest of the thesis. These chiral edges are combinations of armchair and zigzag edges. Several minimal chiral terminations can be seen in figure 2.2.

For any graphene ribbon having a periodic edge, there will be a primitive translation vector leaving the wavefunction invariant up to a phase. We denote this vector by $\mathbf{T}$, and project it into the basis indicated indicated in figure 2.1:

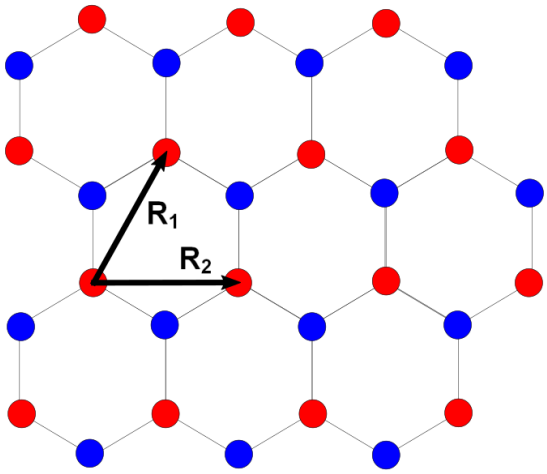

Figure 2.1: Graphene decomposes into two triangular lattices. Primitive translation vectors are indicated.

$$\mathbf{T} = n\mathbf{R}_1 + m\mathbf{R}_2, \tag{2.1}$$

where n and m are non-negative integers. For so-called minimal chiral ribbons, these integers n and m completely determine the ribbon, and they represent the number of respective zigzag and armchair components along the edge of the ribbon unit cell. In the remainder of this thesis we will concentrate on minimal ribbons, using the notation (n, m) to refer to a particular minimal chiral ribbon.

The primitive translation vectors of zigzag and armchair ribbons can be written

$$\mathbf{T}_Z = \mathbf{R}_1 \tag{2.2}$$

$$\mathbf{T}_A = \mathbf{R}_1 + \mathbf{R}_2. \tag{2.3}$$

Comparing with equation 2.1, we see that a zigzag ribbon is a $(1, 0)$ ribbon, while an armchair ribbon is a $(1, 1)$ ribbon. Instead of characterising a given

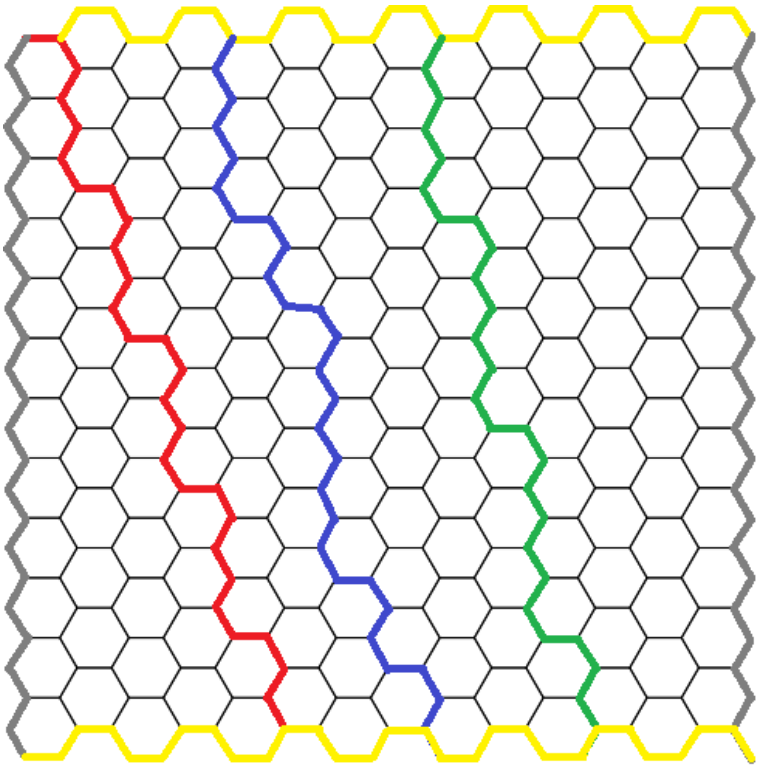

Figure 2.2: A collection of possible minimal edge terminations of graphene. Grey–zigzag; yellow– armchair; red– (2,1) chiral; blue– (3,2) chiral; green– (3,1) chiral.

minimal chiral ribbon by (n, m), we can alternatively use the so-called chiral angle, which is the angle between the translation vector of the (n, m) ribbon and the translation vector of the zigzag ribbon:

$$\theta = \arccos \frac{\mathbf{T} \cdot \mathbf{T}_Z}{|\mathbf{T}||\mathbf{T}_Z|} = \arcsin \sqrt{\frac{3}{4} \frac{m^2}{n^2 + nm + m^2}}. \tag{2.4}$$

This chiral angle ranges between the zigzag limit $\theta = 0$ and the armchair limit $\theta = \pi/6$. We are interested in the intermediate chiralities. The magnitude of the (n, m) translation vector is

$$T = \sqrt{\mathbf{T} \cdot \mathbf{T}} = a\sqrt{n^2 + nm + m^2}. \tag{2.5}$$

We can project the (n, m) translation vector into the basis of zigzag and armchair edges:

$$\mathbf{T} = (n - m)\mathbf{T}_Z + m\mathbf{T}_A. \tag{2.6}$$

This representation will later be useful for describing the electronic structure of chiral ribbons.

2.1 Zigzag and armchair

The two simplest and most-studied graphene ribbons are the zigzag and armchair ribbons. In 1995 Nakata et al. showed that a semi-infinite graphene sheet with a zigzag edge has a band of states localized to the edge with exactly zero energy, while the armchair ribbon has no edge-localized states. [9] Analytic studies of finite-width zigzag graphene ribbons in a non-interacting electron picture have indicated that these edge states persist with confinement, but the two edge states –one at each edge– mix across the ribbon due to their finite overlap, splitting into bonding and anti-bonding states with a quantum confinement gap exponentially small in ribbon width. [14]

This exponential dependence of this gap on zigzag ribbon width is inconsistent with ab initio calculations, and it has been proposed there is an additional contribution to the energy gap due to magnetic ordering on the edges of the graphene ribbon [5] [12]. Edge-localized ferromagnetic ordering was later proven in the local approximation in the limit of small U/t by Karimi and Affleck in 2010 [8]. This proof of magnetism by Karimi and Affleck will be reviewed in chapter 3. We will then apply a generalization of this work to numerically prove edge ferromagnetism on certain chiral ribbons in chapter 4. Armchair ribbons in contrast to zigzag have no low energy localized edge states, and the gap at the Dirac point is due only to quantum confinement in a finite ribbon. There is no edge-localized ferromagnetism.

2.2 Chiral

A minimal chiral ribbon is a ribbon with edges which are a mixture of zigzag and armchair components. Several studies suggest edge states will persist on the zigzag components of the chiral edge, leading to some density of zigzag-like localized edge states near zero energy. Experimentally, these chiral edge states have been seen in the local density of states obtained through scanning tunneling experiments [13]. Theoretically, the existence of chiral edge modes has been proven, and their density has been calculated by a 2D band-structure projection scheme [1]. Additonally, mean-field theory calculations suggest magnetic ordering the edges of minimal chiral graphene ribbons [3] [16].

We would like to predict this magnetic ordering on chiral ribbons by another method, using an edge-projected Hubbard interaction which is valid in a small U/t limit, generalizing the work of Karimi and Affleck on the zigzag ribbon [8]. Using this method we will prove edge ferromagnetism on several particular chiral ribbons.

Chapter 3

Electronic and Magnetic Structure of Zigzag Ribbons

Semi-infinite zigzag ribbons have one localized edge mode per spin on each edge. These flat bands exist across one-third of the Brillouin zone at exactly zero energy. In the first section of this chapter, we will show the existence of these bands and calculate their density. In the second section of this chapter, following [8], we will prove in an edge-projected Hubbard approximation that interactions among these localized edge electrons induce ferromagnetic ordering along the edge in the ground state.

3.1 Electronic structure of zigzag ribbons

In this section we will derive the edge state spectra and wavefunctions on the zigzag ribbon in the limit of semi-infinite width. We will show the edge mode bands are dispersionless at exactly zero energy. These edge mode bands span the Brillouin zone between the so-called Dirac points, where the bulk bands contact the Fermi level with the linear dispersion characteristic of massless Dirac fermions [4] [2].

We will not discuss bulk electronic properties in any detail, as they are not relevant for our present study of edge magnetism. A rough schematic of the band structure of a semi-infinite zigzag ribbon is indicated in figure 3.1.

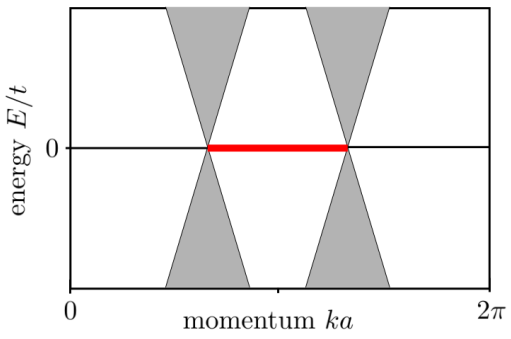

Figure 3.1: A schematic spectrum of the zigzag ribbon with edge mode band highlighted in red and bulk bands in grey.

3.1.1 Zero energy edge states in zigzag ribbons

With nearest neighbour tight-binding hamiltonian

$$H = t \sum_{\langle i,j \rangle} c_i^\dagger c_j + h.c., \tag{3.1}$$

using the unit cell and labeling scheme indicated in figure 3.2, we obtain Schrödinger equation

$$E\alpha_{n,m} = t(\beta_{n-1,m} + \beta_{n,m} + \beta_{n,m+1}) \tag{3.2}$$

$$E\beta_{n,m} = t(\alpha_{n+1,m} + \alpha_{n,m} + \alpha_{n,m-1}). \tag{3.3}$$

Translational invariance over $\mathbf{T}$ invites a crystal momentum $\mathbf{k} \cdot \mathbf{T} = kT$ with $\psi_{\mathbf{r}+\mathbf{T}} = \exp[ikT]\psi_{\mathbf{r}}$, and the Bloch equation is

$$E\alpha_m(k) = t((1 + e^{-ika})\beta_m(k) + \beta_{m+1}(k) \tag{3.4}$$

$$E\beta_m(k) = t((1 + e^{ika})\alpha_m(k) + \alpha_{m-1}(k). \tag{3.5}$$

We would like to find any modes which may exist at exactly zero energy. Notice the two sublattices decouple at zero energy. This occurs generally for more complicated chiral edge terminations as well. Forming the Bloch

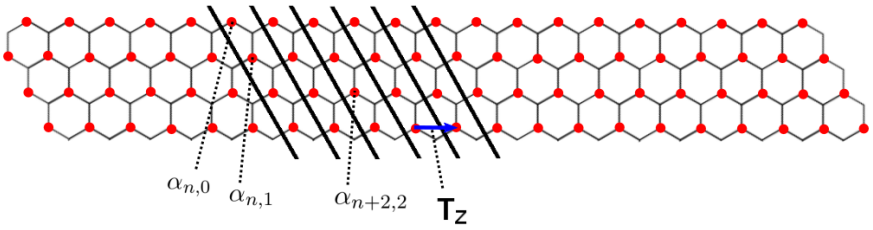

Figure 3.2: A zigzag ribbon segment is shown with the primitive translation vector indicated. One sublattice is highlighted and our choice of unit cell is indicated. Several sites are labeled with their wavefunctions to indicate the $\alpha_{n,m}$ notation. n is the index along the direction of $\mathbf{T}$, while m is the distance away from the upper edge.

equation at $E = 0$ and making an exponential ansatz

$$\alpha_m(k) \propto e^{-ma/\Lambda(k)}, \tag{3.6}$$

(and similarly for $\beta_m(k)$) we find eigenstates

$$\alpha_m(k) = [-2\cos ka/2]^m e^{ikam/2}\alpha_0(k) \tag{3.7}$$

$$\beta_m(k) = [-2\cos ka/2]^{W-1-m} e^{-ikam(W-1-m)/2}\beta_{W-1}(k), \tag{3.8}$$

where the dimensionless width $W - 1$ is the largest value m takes on. We observe that the $\alpha_m(k)$ modes decay exponentially away from the $m = 0$ edge, while the $\beta_m(k)$ decay exponentially away from the $m = W - 1$ edge.

Considering normalizability, we see these exponentially decaying eigenstates are only simultaneous eigenstates in the limit of infinite width $W \to \infty$, which is the limit in which the localized edge modes do not overlap across the ribbon. Because there are no other modes near zero energy these edge states can mix with, in a finite system these two modes will overlap and split into bonding and anti-bonding pairs, gapping the edge-mode spectrum away from $E = 0$ with a gap exponentially small in W [14]. In the semi-infinite limit of large W, the edge modes will be approximately dispersionless zero

energy bands. Since these bands have no curvature, their effective mass is infinite. Electrons in these bands are localized to the edge of the ribbon and are delocalized in the direction along **T**.

From this point onward we concentrate only on semi-infinite ribbons for which W is large enough that there is no mixing across the ribbon. We have two zero energy states (per spin). One on each edge or equivalently one per sublattice. The electron density in these edge modes decays exponentially into the ribbon away from the edge with a characteristic length $\Lambda(k) = -a \ln |2 \cos ka/2|^{-1}$:

$$|\alpha_m(k)| = \sqrt{\frac{2a}{\Lambda(k)}} e^{-ma/\Lambda(k)} |\alpha_0(k)| \tag{3.9}$$

$$|\beta_m(k)| = \sqrt{\frac{2a}{\Lambda(k)}} e^{-(W-1-m)a/\Lambda(k)} |\beta_0(k)|. \tag{3.10}$$

This penetration length diverges in the limits $ka = 2\pi/3$ and $ka = 4\pi/3$– the location of the Dirac points in the zigzag ribbon spectrum. In the finite system, the overlap of the edge modes on opposite edges is largest at values of k for which the correlation length diverges, so we expect the largest finite-size splitting at the Dirac points.

3.1.2 Density of states in zigzag

The density of localized edge states per length of ribbon and per spin in the semi-infinite zigzag ribbon is approximately $1/3a$:

$$\rho(E) = \sum_{2\pi/3<ka<4\pi/3} \delta(E) \approx \int_{2\pi/3a}^{4\pi/3a} \frac{dk}{2\pi} \delta(E) = \frac{1}{3a} \delta(E). \tag{3.11}$$

We see that there is about one edge-localized electron state per 3 unit cells in the zigzag ribbon.

3.2 Magnetic structure of zigzag edge states

In order to understand the low energy magnetic structure of zigzag ribbons, we include local Coulomb repulsion via a Hubbard interaction assumed to be small relative to the non-interacting hamiltonian. We project this interaction into the non-interacting eigenbasis. In the semi-infinite ribbon, the edge and bulk modes will be well separated in energy– the dispersionless edge modes being at exactly zero energy. In the low energy limit therefore only the $E = 0$ bands will be accessible to scattering processes. In this way we can justify neglecting bulk-to-bulk (bulk-bulk) scattering and scattering between bulk modes and edge modes (bulk-edge) [8]. This is the central approximation which allows an analytical understanding of magnetism in zigzag ribbons. This edge-projection scheme supports a rigorous proof of the existence of a unique edge-ferromagnetic ground state, accessible in the limits of $U \ll t$ and semi-infinite width.

3.2.1 Edge-projected Hubbard interactions in zigzag

We seek the ground state of the hamiltonian

$$H = t \sum_{\langle i,j\rangle,\sigma} \{c^\dagger_{i\sigma} c_{j\sigma} + c^\dagger_{j\sigma} c_{i\sigma}\} + H_U - \mu \sum_{i,\sigma} c^\dagger_{i\sigma} c_{i\sigma}, \tag{3.12}$$

where H_U is the Hubbard hamiltonian

$$H_U = U \sum_i c^\dagger_{i\uparrow} c_{i\uparrow} c^\dagger_{i\downarrow} c_{i\downarrow}, \tag{3.13}$$

and the last term is included to preserve particle-hole symmetry.

In this section we will review an appproximation to this interacting problem created by Karimi and Affleck [8] and based on the work of Schmidt and Loss [11], in which we project the interacting problem onto the non-interacting eigenstates and neglect bulk-bulk and bulk-edge interactions in anticipation of an effective theory with all bulk states at negative energy occupied and all bulk states at positive energy unoccupied. Our neglect of bulk-edge interactions will be justified in the limit of $U/t \ll 1$ because

the overlap of localized edge states with delocalized bulk states is small. The neglect of bulk-bulk interactions is justified because the effect of bulk interactions is marginal [10].

We diagonalize the hamiltonian $H = t\sum c^\dagger_{i\sigma}c_{j\sigma} + h.c.$ and obtain a set of non-interacting eigenstates characterized in Bloch space by creation operators $c^\dagger_\sigma(k)$. We partition this set of eigenstates into edge states $e^\dagger_\sigma(k)$ and bulk states $b^\dagger_\sigma(k)$:

$$\{c^\dagger_\sigma(k)\} = \{e^\dagger_\sigma(k)\} \cup \{b^\dagger_\sigma(k)\}. \tag{3.14}$$

Our central approximation is to work in a low energy limit in which bulk-edge and bulk-bulk interactions are insignificant. Projecting 3.13 into this partitioned basis 3.14 we obtain different terms. Some describe scattering processes between edge modes, while others describe scattering processes between edge and bulk or exclusively between bulk modes:

$$\begin{aligned} H_U = &\sum_{k_1k_2k_3k_4} \Gamma(k_1,k_2,k_3,k_4)e^\dagger_\uparrow(k_1)e_\uparrow(k_2)e^\dagger_\downarrow(k_3)e_\downarrow(k_4) \\ &+ \sum_{k_1k_2k_3k_4} \Gamma'(k_1,k_2,k_3,k_4)b^\dagger_\uparrow(k_1)b_\uparrow(k_2)e^\dagger_\downarrow(k_3)e_\downarrow(k_4) + \dots \end{aligned} \tag{3.15}$$

At this point we perform the aforementioned approximations and neglect all but the first term describing scattering only among edge states. We concentrate on a semi-infinite ribbon so that the zero-energy edge wavefunctions take the form

$$\alpha_{n,m}(k) = e^{ika(n+m/2)}[-2\cos ka/2]^m\alpha_0(k) = e^{ikna}\alpha_m(k), \tag{3.16}$$

and the only vertex factor Γ we are concerned with in 3.15 becomes:

$$\begin{aligned}\Gamma(k_1,k_2,k_3,k_4) &= U\sum_{n,m}\alpha^*_{n,m}(k_1)\alpha_{n,m}(k_2)\alpha^*_{n,m}(k_3)\alpha_{n,m}(k_4)\\ &= LU\delta_{k_1-k_2+k_3-k_4}\sum_m \alpha^*_m(k_1)\alpha_m(k_2)\alpha^*_m(k_3)\alpha_m(k_4),\end{aligned} \tag{3.17}$$

where L is the length of the ribbon (the number of unit cells).

Using this interaction function we obtain our edge-projected Hubbard hamiltonian for the zigzag ribbon:

$$H_U = \sum_{kk'q}\Gamma(k,k',q)e^\dagger_\uparrow(k+q)e_\uparrow(k)e^\dagger_\downarrow(k'-q)e_\downarrow(k'). \tag{3.18}$$

Here

$$\begin{aligned}&\Gamma(k,k',q) = LU\sum_m \alpha^*_m(k+q)\alpha_m(k)\alpha^*_m(k'-q)\alpha_m(k')\\ &= LU\frac{\{\big[1-4\cos^2\frac{(k+q)a}{2}\big]\big[1-4\cos^2\frac{ka}{2}\big]\big[1-4\cos^2\frac{(k'-q)a}{2}\big]\big[1-4\cos^2\frac{k'a}{2}\big]\}^{1/2}}{1-16\cos\frac{(k+q)a}{2}\cos\frac{ka}{2}\cos\frac{(k'-q)a}{2}\cos\frac{k'a}{2}}.\end{aligned} \tag{3.19}$$

The sum over k, k' and q is restricted to the band in which $2\pi/3 < (k+q)a, ka, (k'-q)a, k'a < 4\pi/3$. Incorporating the energy shift $-\mu\sum_{k,\sigma}e^\dagger_\sigma(k)e_\sigma(k)$ into the Hubbard hamiltonian to restore particle-hole symmetry, the edge-projected Hubbard hamiltonian takes the form

$$H_U = \sum_{kk'q}\Gamma(k,k',q)\big[\sum_\sigma e^\dagger_\sigma(k+q)e_\sigma(k)-\delta_{q=0}\big]\big[\sum_{\sigma'}e^\dagger_{\sigma'}(k'-q)e_{\sigma'}(k')-\delta_{q=0}\big]. \tag{3.20}$$

Introducing the operators $O_m(q)$ and $O^\dagger_m(q)$ defined by

$$O^\dagger_m(q) = \sqrt{LU}\sum_k \alpha^*_m(k+q)\alpha_m(k)\big[\sum_\sigma e^\dagger_\sigma(k+q)e_\sigma(k)-\delta_{q=0}\big], \tag{3.21}$$

the Hubbard hamiltonian takes positive definite form

$$H_U = \sum_{q,m} O_m^\dagger(q) O_m(q). \tag{3.22}$$

In this form it is obvious that the ground state of our hamiltonian has $E = 0$. One can see that a fully spin-polarized state is a zero energy state and therefore a ground state. Consider for example a state with spin up electrons at every momentum k. It is clear that $O_m(q)$ annihilates this state, because the spin-up terms in $O_m(q)$ try to create a spin-up electron with momentum $k + q$ in an occupied fermionic state, and the spin-down terms in $O_m(q)$ try to annihilate a spin-down electron with momentum k in an unoccupied state. It remains to show that this ferromagnetic ground state is also unique.

3.2.2 Uniqueness of ferromagnetic ground state in zigzag

We now argue that the two fully polarized multiplets of total spin $S = L/6$ are the unique ground states of 3.12 in our edge-projected approximation. In order to prove this uniqueness, we need only show that the only ground states annihilated by the operator $O_m(q)$ for all m and q are fully polarized, i.e. they have maximal total spin. This means the ground state wavefunction is only expressible as a symmetric combination of Fock states with a single occupancy at each momentum.

Assume that $|\psi\rangle$ is annihilated by $O_m(q)$ for all m and q. In symbols,

$$\begin{aligned} 0 &= O_m(q)|\psi\rangle \\ &\propto \sum_k \alpha_m^*(k)\alpha_m(k+q)\big[\sum_\sigma e_\sigma^\dagger(k+q)e_\sigma(k) - \delta_{q=0}\big]|\psi\rangle. \end{aligned} \tag{3.23}$$

We argue in the Appendix 5 using the Vandermonde theorem that equation 3.25 implies the following condition which we will apply repeatedly in order to prove ferromagnetism in the ground state:

$$0 = \big[\sum_{\sigma}\{e^{\dagger}_{\sigma}(k+q)e_{\sigma}(k) + e^{\dagger}_{\sigma}(-k)e_{\sigma}(-k-q)\} - 2\delta_{q=0}\big]|\psi\rangle. \tag{3.24}$$

In particular, let us choose this equation with $q = 0$. Then we have

$$0 = \big[\sum_{\sigma}\{e^{\dagger}_{\sigma}(k)e_{\sigma}(k) + e^{\dagger}_{\sigma}(-k)e_{\sigma}(-k)\} - 2\big]|\psi\rangle. \tag{3.25}$$

This equation is satisfied if and only if $|\psi\rangle$ is such that

$$\big[n(k) + n(-k)\big]|\psi\rangle = 2|\psi\rangle \tag{3.26}$$

for all k. Here $n(k) = \sum_{\sigma=\uparrow,\downarrow} e^{\dagger}_{\sigma}(k)e_{\sigma}(k)$ is the number operator for the edge state at momentum k. This restriction leaves us two options for the occupation of momentum states $-k$ and k: Either $n(k) = n(-k) = 1$, or $n(-k) = 0$ and $n(k) = 2$ (or vice-versa). We call the second possibility an excition. Now we will prove that excitons are not permitted in the ground state of the hamiltonian 3.22.

In general, any state $|\psi\rangle$ may be represented as a linear combination of all possible Fock states

$$\prod_{k,\sigma} e^{\dagger}_{\sigma}(k)|0\rangle. \tag{3.27}$$

Here the product can run over any subset of the momenta k and spins σ supporting edge modes: $2\pi/3 < |ka| < 4\pi/3$, of which there are approximately $L/3$. Consider a state $|\phi\rangle$ satisfying $n(k) + n(-k) = 2$ for all k with an exciton arbitrarily placed at momentum l. We write this as

$$|\phi\rangle = |\ldots, \underbrace{0}_{-l}, \ldots, \underbrace{\downarrow\uparrow}_{l}, \ldots\rangle. \tag{3.28}$$

We assume this excitonic state $|\phi\rangle$ may enter the Fock state expansion of our ground state $|\psi\rangle$. That is, we assume $\langle\phi|\psi\rangle \neq 0$. Now seeking a contradiction we impose condition 3.24 on $|\psi\rangle$ with the particular choice of $q = -2l$ and

$k = l$. We should then have

$$\sum_{\sigma} e_{\sigma}^{\dagger}(-l)e_{\sigma}(l)|\psi\rangle = 0. \tag{3.29}$$

Since we assume the excitonic state $|\phi\rangle$ enters the expansion of our ground state $|\psi\rangle$, we are led to consider the action of this operator $\sum_{\sigma} e_{\sigma}^{\dagger}(-l)e_{\sigma}(l)$ on $|\phi\rangle$:

$$\begin{aligned}\sum_{\sigma} e_{\sigma}^{\dagger}(-l)e_{\sigma}(l)|\ldots,\underbrace{0}_{-l},\ldots,\underbrace{\downarrow\uparrow}_{l},\ldots\rangle \\ = |\ldots,\underbrace{\uparrow}_{-l},\ldots,\underbrace{\downarrow}_{l},\ldots\rangle - |\ldots,\underbrace{\downarrow}_{-l},\ldots,\underbrace{\uparrow}_{l},\ldots\rangle\end{aligned} \tag{3.30}$$

Clearly, this operator acting on $|\psi\rangle$ gives a non-zero contribution. Therefore in order to satisfy the condition 3.29 there must be some other states in the Fock state representation of the ground state $|\psi\rangle$ which together cancel the excitonic state $|\phi\rangle$'s non-zero contribution in 3.30. Since the operator $\sum_{\sigma} e_{\sigma}^{\dagger}(-l)e_{\sigma}(l)$ only connects momenta l and $-l$, all other momenta are unchanged by the operator and there are only three other states which could cancel the terms generated from the excitonic state $|\phi\rangle$ in 3.30:

$$|1\rangle = |\ldots,\underbrace{\uparrow\downarrow}_{-l},\ldots,\underbrace{0}_{l},\ldots\rangle \qquad \textstyle\sum_{\sigma} e_{\sigma}^{\dagger}(-l)e_{\sigma}(l)|1\rangle = 0 \tag{3.31}$$

$$|2\rangle = |\ldots,\underbrace{\uparrow}_{-l},\ldots,\underbrace{\downarrow}_{l},\ldots\rangle \qquad \textstyle\sum_{\sigma} e_{\sigma}^{\dagger}(-l)e_{\sigma}(l)|2\rangle = |1\rangle \tag{3.32}$$

$$|3\rangle = |\ldots,\underbrace{\downarrow}_{-l},\ldots,\underbrace{\uparrow}_{l},\ldots\rangle \quad \textstyle\sum_{\sigma} e_{\sigma}^{\dagger}(-l)e_{\sigma}(l)|3\rangle = -|1\rangle. \tag{3.33}$$

Since $\sum_{\sigma} e_{\sigma}^{\dagger}(-l)e_{\sigma}(l)|\phi\rangle = |2\rangle - |3\rangle$, and none of the three possible states map through $\sum_{\sigma} e_{\sigma}^{\dagger}(-l)e_{\sigma}(l)$ into $|2\rangle$ or $|3\rangle$, the terms generated by the excitonic state in 3.30 cannot be canceled by any other allowed kets in the Fock state expansion of the ground state, and therefore $\langle\phi|\psi\rangle = 0$. That is,

we've contradicted the assumption that there is an excitonic contribution to ground state wavefunction of the edge-projected Hubbard hamiltonian. We've now narrowed down the possible states in the Fock state expansion of the ground state to states with $n(k) = n(-k) = 1$ at all momenta k. There are no excitions allowed in the ground state.

Having shown there are no excitonic states, we now show that the allowed states with $n(k) = n(-k) = 1$ for all k in the Fock state expansion of the ground state $|\psi\rangle$ always enter symmetrically like

$$|\ldots, \underbrace{\uparrow}_{k}, \ldots, \underbrace{\downarrow}_{k'}, \ldots\rangle + |\ldots, \underbrace{\downarrow}_{k}, \ldots, \underbrace{\uparrow}_{k'}, \ldots\rangle \tag{3.34}$$

and never anti-symmetrically like

$$|\ldots, \underbrace{\uparrow}_{k}, \ldots, \underbrace{\downarrow}_{k'}, \ldots\rangle - |\ldots, \underbrace{\downarrow}_{k}, \ldots, \underbrace{\uparrow}_{k'}, \ldots\rangle. \tag{3.35}$$

To see this, consider the constraint 3.24 again but with $q = k' - k$. We have

$$\sum_{\sigma} \left[e^{\dagger}_{\sigma}(k')e_{\sigma}(k) + e^{\dagger}_{\sigma}(-k)e_{\sigma}(-k')\right]|\psi\rangle = 0. \tag{3.36}$$

Now assume the expansion of $|\psi\rangle$ has a state like $|\ldots, \underbrace{\uparrow}_{k}, \ldots, \underbrace{\downarrow}_{k'}, \ldots\rangle$ in it. The action of the operator in 3.36 is

$$\sum_{\sigma} \left[e^{\dagger}_{\sigma}(k')e_{\sigma}(k) + e^{\dagger}_{\sigma}(-k)e_{\sigma}(-k')\right]|\ldots, \underbrace{\uparrow}_{k}, \ldots, \underbrace{\downarrow}_{k'}, \ldots\rangle$$
$$= |\ldots, \underbrace{0}_{k}, \ldots, \underbrace{\downarrow\uparrow}_{k'}, \ldots\rangle. \tag{3.37}$$

We also have

$$\sum_{\sigma}\left[e_{\sigma}^{\dagger}(k')e_{\sigma}(k)+e_{\sigma}^{\dagger}(-k)e_{\sigma}(-k')\right]|\ldots,\underbrace{\downarrow}_{k},\ldots,\underbrace{\uparrow}_{k'},\ldots\rangle$$
$$=-|\ldots,\underbrace{0}_{k},\ldots,\underbrace{\downarrow\uparrow}_{k'},\ldots\rangle. \quad (3.38)$$

Since 3.36 must hold, it's clear that states must enter symmetrically into the Fock state expansion of the ground state $|\psi\rangle$. Therefore, we have found our ground state $|\psi\rangle$ is a symmetric combination of Fock states with a single occupancy at each momentum. These allowed ground states are then all SU(2) rotations of the fully polarized states $|\uparrow,\uparrow,\uparrow,\ldots\rangle$ (and spin-down) with total spin $S \approx L/6$. This completes the proof of ferromagnetism in the edge states of the zigzag ribbon in the $U/t \ll 1$ limit.

3.3 Summary of electronic and magnetic properties of zigzag

Zigzag ribbons have been shown to manifest a density of edge-localized states at exactly zero energy in the limit of semi-infinite width [4]. Using an edge-projected Hubbard interaction, we have argued following Karimi and Affleck in [8] that a small on-site Coulomb repulsion drives a ferromagnetic ordering of electrons localized at the edge in these dispersionless zero energy states. In the next chapter we will apply a generalization of this argument for ferromagnetism to certain chiral ribbons.

Chapter 4

Electronic and Magnetic Structure of Chiral Ribbons

Chiral ribbons are known experimentally to manifest edge states from STM and STS experiments [13]. It has been established that there is always some enhancement of the local density of states due to edge-localized states for all carbon ribbon edge terminations except for armchair [1]. Several authors have studied an appropriate Hubbard model in the mean field approximation and have found ferromagnetic edge state ordering in chiral ribbons [16] [3] [6]. We would like to clarify these findings by calculating edge mode spectra and showing ferromagnetic ordering in the chiral edge state by a means other than mean field theory.

4.1 Electronic structure of chiral ribbons

The band structure of any minimal graphene ribbon can be obtained from projecting the two-dimensional band structure of graphene onto an appropriate direction. This projection has been used to derive the density of zero energy edge states per length and per spin on semi-infinite chiral ribbons [1]. The result is

$$\rho(\theta) = \frac{2}{3a}\cos(\theta + \pi/3), \tag{4.1}$$

where θ is the chiral angle which ranges between 0 for zigzag and $\pi/6$ for armchair. We can see the density of edge states decreases as more armchair components are incorporated into the primitive translation vector. In low chirality ribbons with a large ratio of zigzag to armchair links, the edge mode

bands can become degenerate, with more than one localized edge state at a given momentum. One group has performed many numerical chiral ribbon band structure calculations, and they have created a scheme to predict the degeneracy of edge mode bands from a band-folding argument [7]. Though these rules do not appear to have a rigorous foundation, we have found them consistent with every case we've checked. In the next section, we will review this band-folding conjecture.

4.1.1 Degeneracy of chiral edge mode bands

The band folding conjecture of Jaskólski et al. allows one to predict the degeneracy of chiral edge mode bands without performing calculations. Their claim is this: The edge mode spectrum of an (n, m) chiral ribbon is the same as the edge mode spectrum of an $(n - m, 0)$ zigzag ribbon. This supports a belief that chiral zero mode properties are determined only by the zigzag segments in the chiral unit cell, and not by armchair segments.

The (n, m) chiral translation vector is

$$\mathbf{T}_{n,m} = (n - m)\mathbf{T}_Z + m\mathbf{T}_A, \tag{4.2}$$

where the basis is defined in equation 2.2. This decomposition is indicated for the particular case of a $(2, 1)$ ribbon in figure 4.2. We see there are $n - m$ zigzag links in the (n, m) chiral unit cell. Jaskólski et al. report from their numerical calculations that the zero mode spectrum of the (n, m) chiral ribbon is identical to the zero mode spectrum of the zigzag ribbon with its unit cell enlarged artificially by a factor of $S = n - m$, i.e. an $(S, 0)$ ribbon. Therefore, let us determine the edge mode spectrum of an $(S, 0)$ ribbon.

With translation vector $S\mathbf{T}_Z$, the first Brillouin zone has extent $|k| \leq \pi/aS$. We know the edge mode spectrum in an extended zone scheme with $|k| < \pi/a$ from our previous calculations in chapter 3. We can then fold the bands from higher zones into our first Brillouin zone $|k| \leq \pi/aS$ to obtain the band structure of the $(S, 0)$ ribbon. This process is indicated in the top panels of figure 4.1. Depending on $S = n - m$, the zero energy bands

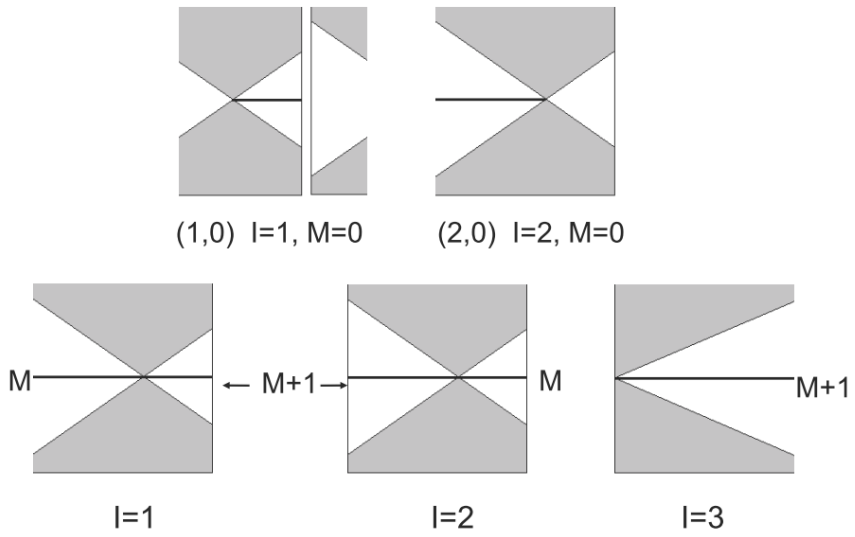

Figure 4.1: From [7]– Schematic band structures of zigzag (1,0), (2,0) and general (S,0) edges after folding the (1,0) zigzag edge band, where $S = I + 3M$. The shaded areas represent bulk states. Degeneracies of zero-energy bands $(M, M + 1)$ are indicated in the lower panels.

resulting from this folding process may become degenerate, with multiple zero energy states at a given momentum. The two Dirac points of the bulk bands can also become degenerate. Whenever this Dirac degeneracy occurs, zero energy bands will span the entire Brillouin zone. If the Dirac points are non-degenerate, zero energy bands will span the segments of the Brillouin zone between the Dirac points.

The result of folding for a given S is summarized by the following relationship: $S = I + 3M$, where $I = 1, 2, 3$ and $M = 0, 1, 2, ...$; if $I = 1$ or 2 in this decomposition of S, the Dirac points are non-degenerate. If $I = 3$, they're degenerate. M then determines the degeneracy of the edge mode bands according to the lower panels of figure 4.1.

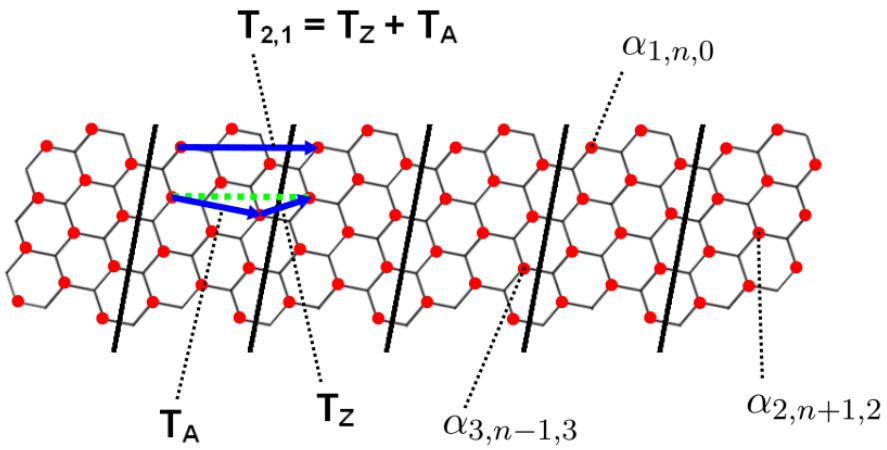

Figure 4.2: One division into unit cells and the decomposition of the primitive translation vector for the $(2,1)$ ribbon into zigzag and armchair components. Several sites are labeled with their wavefunction to indicate the labeling scheme on the $(2,1)$ ribbon.

4.1.2 (2,1) chiral ribbon edge mode structure

The $(2,1)$ ribbon has translation vector $\mathbf{T}_{2,1} = \mathbf{T}_Z + \mathbf{T}_A$. The magnitude of this translation vector is $T = a\sqrt{7}$. Its chiral angle (eq. 2.4) is $\theta_{2,1} = 19.1°$. Since the (2,1) ribbon has one zigzag component per unit cell, following [7] and noting $2-1 = 3(0)+1$, we expect a single band of zero energy states (per spin) extending between the Dirac points at $kT = 2\pi/3$ and $kT = 4\pi/3$.

We divide the $(2,1)$ ribbon into unit cells as shown in figure 4.2. We label the wavefunction on a given site as $\alpha_{i,n,m}$. Here n labels the unit cell. $m = 0, 1, 2, ...$ labels the distance away from the upper edge in each unit cell, and $i = 1, 2, 3$ labels the three distinct sites at each m within the unit cell. At zero energy the two sublattices of the graphene ribbon decouple. Nearest neighbour hopping on the $(2,1)$ ribbon leads to the following for the lattice Schrödinger equation on one of the two sublattices at zero energy. The other sublattice is accessible by inversion.

$$0 = \alpha_{1,n,m} + \alpha_{2,n,m} + \alpha_{2,n,m+1} \tag{4.3}$$

$$0 = \alpha_{2,n,m} + \alpha_{3,n,m} + \alpha_{3,n,m+1} \tag{4.4}$$

$$0 = \alpha_{3,n,m} + \alpha_{1,n+1,m} + \alpha_{1,n+1,m-1}. \tag{4.5}$$

Translational invariance along $\mathbf{T}$ invites the use of Bloch's theorem $\alpha_{i,n,m} = e^{iknT}\alpha_{i,m}(k)$, where T is the magnitude of the primitive translation vector on the ribbon. The Bloch equations are

$$\alpha_{1,m} + \alpha_{2,m} + \alpha_{2,m+1} = 0 \tag{4.6}$$

$$\alpha_{2,m} + \alpha_{3,m} + \alpha_{3,m+1} = 0 \tag{4.7}$$

$$e^{-ikT}\alpha_{3,m} + \alpha_{1,m} + \alpha_{1,m-1} = 0. \tag{4.8}$$

These equations only hold away from the edge. The boundary condition at the edge is

$$0 = \alpha_{1,m=0} + \alpha_{2,m=1}. \tag{4.9}$$

We also require that the wavefunctions must be normalizable:

$$\sum_{i=1}^{3}\sum_{m=0}^{\infty} |\alpha_{i,m}(k)|^2 = 1. \tag{4.10}$$

Making an exponential ansatz $\alpha_{1,m}(k) \propto \nu(k)^m$ in the Bloch equations 4.6 to 4.8 provides a secular equation for the roots $\nu(k)$:

$$\nu(k)^3 + 3\nu(k)^2 + (3 + e^{-ikT})\nu(k) + 1 = 0. \tag{4.11}$$

Note the appearance of the binomial coefficients $1, 3, 3, 1$. This equation has three complex roots $\nu_1(k), \nu_2(k), \nu_3(k)$ which we can find numerically. Imposing the normalization condition, we find two of the roots are normalizable for $2\pi/3 < |kT| < \pi$, while the third is not normalizable at any k Let us denote the two normalizable roots $\nu_1(k)$ and $\nu_2(k)$.

We've found our expected single zero energy mode wavefunctions which

are non-zero on $2\pi/3 < |kT| < \pi$ (one-third of the Brillouin zone) with the form

$$\alpha_{i,n,m}(k) = e^{iknT}\left[g_i(k)\nu_1(k)^m + l_i(k)\nu_2(k)^m\right], \tag{4.12}$$

where $i = 1, 2, 3$ and the $g_i(k)$, $l_i(k)$ are phase factors fully determined in terms of the $\nu_i(k)$ by the boundary and normalization conditions. These three wavefunctions at each m and k describe a density of electrons at exactly zero energy which decays away from the (2,1) chiral edge exponentially. This density is

$$\rho(\theta_{2,1}) \approx \int_{2\pi/3T}^{4\pi/3T} \frac{dk}{2\pi} = \frac{1}{3a}\frac{1}{\sqrt{7}}. \tag{4.13}$$

We see the $(2,1)$ edge mode density is suppressed by a factor of $1/\sqrt{7} \approx 0.38$ from zigzag. This result agrees with that obtained from equation 4.1 from ref. [1] using $\theta_{2,1} = 19.1°$. Later in this chapter we demonstrate that the form of these zero energy edge modes supports ferromagnetic ordering at the edge of the $(2,1)$ ribbon.

4.1.3 (s,1) chiral ribbon edge mode structure

Extending the calculation to (s,1) ribbons, where s is an arbitrary integer larger than 1, since there are $s-1$ zigzag links, we expect following [7] that the degeneracy and location of the Dirac points are determined by M and I in $s-1 = 3I+M$ which follows from the band-folding scheme those authors present. The translation vector is given by $\mathbf{T} = (n-1)\mathbf{T}_Z + \mathbf{T}_A$ and its magnitude is $T = a\sqrt{s^2+s+1}$.

The $s+1$ lattice Bloch equations at each choice of m on the upper edge's sublattice, using an extension of the unit cell and labeling scheme indicated for the (2,1) ribbon in figure 4.2, are

$$0 = \alpha_{1,m} + \alpha_{2,m} + \alpha_{2,m+1} \tag{4.14}$$

$$0 = \alpha_{2,m} + \alpha_{3,m} + \alpha_{3,m+1} \tag{4.15}$$

$$\vdots \tag{4.16}$$

$$0 = \alpha_{s,m} + \alpha_{s+1,m} + \alpha_{s+1,m+1} \tag{4.17}$$

$$0 = e^{-ikT}\alpha_{s+1,m} + \alpha_{1,m-1} + \alpha_{1,m}. \tag{4.18}$$

The boundary condition is

$$\alpha_{s-1,0} + \alpha_{s,1} = 0. \tag{4.19}$$

We again make the ansatz of an exponentially decaying wave-function into the lattice Bloch equations: $\alpha_{1,m} \propto \nu(k)^m$, which provides a secular equation of $s+1$ order:

$$\begin{aligned} 0 = \binom{s+1}{0}\nu(k)^{s+1} + \binom{s+1}{1}\nu(k)^s + \ldots + \binom{s+1}{s-1}\nu(k)^2 \\ +\{\binom{s+1}{s} + (-1)^s e^{-ikT}\}\nu(k)^1 + \binom{s+1}{s+1}. \end{aligned} \tag{4.20}$$

Solving this equation numerically for many different values of s we find that the normalizable solutions are consistent in every case checked with the degeneracy predicition rules posited in ref. [7]. For example, if $s = 16$ we have fifteen zigzag links in the unit cell so that $15 = I + 3M$ with $I = 3$ and $M = 4$. The folding rules of Jaskólski et al. then indicate we should have a 5-fold degenerate zero energy band across the entire Brillouin zone. We find equation 4.20 has 7 solutions with $|\nu(k)| < 1$ across the entire Brillouin zone. The wavefunctions then have seven undetermined coefficients. Since we have one boundary condition and one normalization condition, we are left with five undetermined coefficients in the wavefunction, which is consistent with a degeneracy of five across the whole Brillouin zone. Other cases of $(s, 1)$ ribbons check out against the folding rules of Jaskólski et al. similarly. We

also find the density of zero modes for all $(s, 1)$ ribbons we have investigated to be in agreement with the Akhmerov et al. result 4.1 with chiral angle calculated by equation 2.4.

4.2 Magnetic structure of chiral ribbons

We have found a general proof of magnetism on chiral ribbons inaccessible thus far. Though minimal chiral ribbons certainly do support localized edge modes of known density and degeneracy, their wavefunctions cannot be known in closed form due to our inability to solve secular equations such as eq. 4.20 exactly. The degeneracy of chiral edge bands is an additional difficulty. This degeneracy introduces arbitrary coefficients into the zero energy wavefunctions. Because we need to invert matrices of arbitary size involving products of these wavefunctions in order to prove magnetism, these arbitrary coefficients lead to a generally intractable problem.

We have however numerically proven edge ferromagnetism on several ribbons with non-degenerate edge modes by generalizing the edge-projected Hubbard scheme developed on zigzag. These numerical calculations show magnetism on ribbons of a fixed length. We have calculated ferromagnetic edge ordering for many diferent ribbon lengths, and this suggests this ordering is a general property independent of length.

4.2.1 (2,1) magnetism

The $(2, 1)$ ribbon has a single edge state per spin extending across one-third of its Brillouin zone, exactly like the zigzag ribbon. Our method of showing edge ferromagnetism proceeds in exact analogy with the zigzag ribbon, except one step of the mathematics is more complicated and cannot be done analytically as before. The process is this: First, we project the Hubbard interaction into the non-interacting eigenbasis and drop bulk-bulk and edge-bulk terms on the basis of $U \ll t$. Second, we argue the unique ground states of this edge-projected Hubbard hamiltonian are fully polarized.

The real space wavefunctions are

$$\begin{aligned}\alpha_{i,n,m}(k) &= e^{iknT}\left[g_i(k)\nu_1(k)^m + l_i(k)\nu_2(k)^m\right] \\ &= e^{iknT}\alpha_{i,m}(k),\end{aligned} \tag{4.21}$$

where $T = a\sqrt{7}$ is the magnitude of the primitive translation vector and the $g_i(k)$ and $l_i(k)$ are phase factors fully determined by boundary and normalization conditions in terms of the two normalizable roots $\nu_1(k)$ and $\nu_2(k)$ of the secular equation 4.11. Here there are four distinct sites per unit cell at a given distance m away from the edge, so $i = 1, 2, 3, 4$.

In the limit $U/t \ll 1$ we can make the approximate transformation $e_\sigma(k) \approx \sum_{i,n,m} \alpha_{i,n,m}(k) c_{(i,n,m)\sigma}$ which corresponds to neglecting bulk-bulk and edge-bulk interactions, so that

$$\begin{aligned}H_U &= U \sum_{i,n,m} c^\dagger_{(i,n,m)\uparrow} c_{(i,n,m)\uparrow} c^\dagger_{(i,n,m)\downarrow} c_{(i,n,m)\downarrow} \\ &\approx U \sum_{i,n,m} \sum_{k_1 k_2 k_3 k_4} \alpha_{i,n,m}(k_1)\alpha^*_{i,n,m}(k_2)\alpha_{i,n,m}(k_3)\alpha^*_{i,n,m}(k_4) \\ &\qquad \times e^\dagger_\uparrow(k_1) e_\uparrow(k_2) e^\dagger_\downarrow(k_3) e_\downarrow(k_4).\end{aligned} \tag{4.22}$$

Noting that

$$\begin{aligned}&\sum_n \alpha_{i,n,m}(k_1)\alpha^*_{i,n,m}(k_2)\alpha_{i,n,m}(k_3)\alpha^*_{i,n,m}(k_4) \\ &\qquad = L\delta_{k_1 - k_2 + k_3 - k_4 = 0}\alpha_{i,m}(k_1)\alpha^*_{i,m}(k_2)\alpha_{i,m}(k_3)\alpha^*_{i,m}(k_4)\end{aligned} \tag{4.23}$$

and renaming the momenta, equation 4.22 takes a form exactly analogous to the Hubbard hamiltonian from the zigzag case equation 3.18:

$$H_U \approx \sum_{kk'q} \Gamma(k, k', q) e^\dagger_\uparrow(k+q) e_\uparrow(k) e^\dagger_\downarrow(k'-q) e_\downarrow(k'), \tag{4.24}$$

where $\Gamma(k, k', q)$ is defined by

$$\Gamma(k,k',q) = LU \sum_{i,m} \alpha_{i,m}(k+q)\alpha^*_{i,m}(k)\alpha_{i,m}(k'-q)\alpha^*_{i,m}(k'). \tag{4.25}$$

In imitation of the zigzag case we now define the operators

$$O^\dagger_{i,m}(q) = \sqrt{LU} \sum_k \alpha^*_{i,m}(k+q)\alpha_{i,m}(k)\big[\sum_\sigma e^\dagger_\sigma(k+q)e_\sigma(k) - \delta_{q=0}\big], \tag{4.26}$$

so that the Hubbard hamiltonian takes the positive definite form

$$H_U = \sum_{i,m,q} O^\dagger_{i,m}(q)O_{i,m}(q). \tag{4.27}$$

Here $i = 1, 2, 3$ is a sum over inequivalent sites at a distance m away from the edge.

We see again that a fully polarized state is a zero energy ground state. From here, in order to show this ferromagnetic ground state is the only possibility, we must show as in the zigzag case that the only states annihilated by $O_{i,m}(q)$ at every q, m, and i are fully polarized. Suppose $O_{i,m}(q)$ annihilates a ground state $|\psi\rangle$. We have

$$0 = \sum_k \alpha^*_{i,m}(k+q)\alpha_{i,m}(k)\big[\sum_\sigma e^\dagger_\sigma(k+q)e_\sigma(k) - \delta_{q=0}\big]|\psi\rangle. \tag{4.28}$$

Again we shift the momenta in the sum by π and choose $q \leq 0$, putting k in the convenient range $-\pi/3 - qT < kT < \pi/3$, and we note that $\alpha^*_{i,m}(k+q)\alpha_{i,m}(k) = \alpha^*_{i,m}(-k)\alpha_{i,m}(-k-q)$. We split the sum in 4.28 into two equal halves $-\pi/3 - qT < kT \leq -qT/2$ and $-qT/2 \leq kT < \pi/3$ and restrict our sum to the upper half at the expense of writing two terms:

$$0 = \sum_{-qT/2 \leq kT < \pi/3} \alpha^*_{i,m}(k+q)\alpha_{i,m}(k) \times \big[\sum_\sigma \{e^\dagger_\sigma(k+q)e_\sigma(k) + e^\dagger_\sigma(-k)e_\sigma(-k-q)\} - 2\delta_{q=0}\big]|\psi\rangle. \quad (4.29)$$

Now we argue that the summand vanishes term by term at every k. Had we the resulting condition

$$\big[\sum_\sigma \{e^\dagger_\sigma(k+q)e_\sigma(k) + e^\dagger_\sigma(-k)e_\sigma(-k-q)\} - 2\delta_{q=0}\big]|\psi\rangle = 0, \quad (4.30)$$

exactly analogous with the zigzag case's equation 3.24, the ferromagnetism proof would follow immediately.

In the zigzag case we argued that the summand vanished at each k by demonstrating the invertibility of a matrix with the Vandermonde theorem, equation 6 in the Appendix. This hinged upon the zigzag wavefunctions having an exponentially decaying form with m. An additional complication with the $(2,1)$ ribbon is that the wavefunctions decay bi-exponentially with m. This removes our ability to use the Vandermonde theorem because the matrix which we need to invert becomes a sum of four Vandermonde matrices, and the determinant of a sum of matrices does not necessarily relate to the determinants of the individual matrices in the sum. However, we still need to show 4.30 holds to prove ferromagnetism of the edge state.

To this end, we fix the length of the ribbon to be L unit cells, thereby fixing the number $D+1$ of momenta on the range $-qT/2 \leq kT < \pi/3$ to be at most $L/6+1$, and we construct a matrix by collating equation 4.29 at the first $D+1$ values of m:

$$\begin{bmatrix} M^i_{0,k_0}(q) & M^i_{0,k_1}(q) & \dots & M^i_{0,k_D}(q) \\ M^i_{1,k_0}(q) & M^i_{1,k_1}(q) & \dots & M^i_{1,k_D}(q) \\ \vdots & \ddots & \ddots & \vdots \\ M^i_{D,k_0}(q) & M^i_{D,k_1}(q) & \dots & M^i_{D,k_D}(q) \end{bmatrix} \begin{bmatrix} |\psi^q_{k_0}\rangle \\ |\psi^q_{k_1}\rangle \\ \vdots \\ |\psi^q_{k_D}\rangle \end{bmatrix} = \begin{bmatrix} 0 \\ 0 \\ \vdots \\ 0 \end{bmatrix}. \tag{4.31}$$

Here the matrix elements are defined by

$$M^i_{m,k}(q) = \alpha^*_{i,m}(k+q)\alpha_{i,m}(k), \tag{4.32}$$

and the kets by

$$|\psi^q_k\rangle = \big[\sum_\sigma \{e^\dagger_\sigma(k+q)e_\sigma(k) + e^\dagger_\sigma(-k)e_\sigma(-k-q)\} - 2\delta_{q=0}\big]|\psi\rangle. \tag{4.33}$$

In order to derive the condition 4.30 from which ferromagnetism follows, we need to show this matrix is invertible. Generally, there is no clear way to do this. However, we have calculated the determinant of this matrix at every q numerically for each choice of $i = 1, 2, 3$ and for system sizes up to $L = 192$– making at most a 32×32 matrix. The determinant is non-zero and therefore we have proven the matrix in question is invertible in every case checked. Therefore it holds for $L \leq 192$ that

$$\big[\sum_\sigma \{e^\dagger_\sigma(k+q)e_\sigma(k) + e^\dagger_\sigma(-k)e_\sigma(-k-q)\} - 2\delta_{q=0}\big]|\psi\rangle = 0. \tag{4.34}$$

From this relationship it follows by exact recapitulation of the steps outlined between equations 3.25 to 3.38 that the ground state of the $(2, 1)$ ribbon is ferromagnetically ordered at the edge. We have thus numerically proven ferromagnetism of the edge state for $L \leq 192$. We expect this magnetism is also plausible for $L > 192$.

4.2.2 (3,1) magnetism

Our analysis of magnetism in the $(3,1)$ chiral ribbon is closely analogous to that used on the $(2,1)$-chiral and $(1,0)$-zigzag ribbons. Following the Jaskólski et al. band-folding argument, noting $3-1=2=I+3M$ with $I=2$ and $M=0$, we expect (see figure 4.1) a single non-degenerate band of zero energy edge modes extending along $-2\pi/3 < kT < 2\pi/3$, where $T=a\sqrt{13}$. This is two-thirds of the Brillouin zone.

The lattice Bloch equations at zero energy are

$$\alpha_{1,m}+\alpha_{2,m}+\alpha_{2,m+1}=0 \tag{4.35}$$

$$\alpha_{2,m}+\alpha_{3,m}+\alpha_{3,m+1}=0 \tag{4.36}$$

$$\alpha_{3,m}+\alpha_{4,m}+\alpha_{4,m+1}=0 \tag{4.37}$$

$$e^{-ikT}\alpha_{4,m}+\alpha_{1,m-1}+\alpha_{1,m}=0, \tag{4.38}$$

and with the ansatz $\alpha_{1,m}(k)\propto\nu(k)^m$ they yield the secular equation (compare with equation 4.20)

$$\nu(k)^4+4\nu(k)^3+6\nu(k)^2+\{4-e^{-ikT}\}\nu(k)+1=0. \tag{4.39}$$

This equation has four complex roots which can be found numerically. Two of the four are normalizable with $|\nu_i(k)|<1$ along the range $-2\pi/3<kT<2\pi/3$ in agreement with the Jaskólski band-folding prediction. The density of zero modes is then

$$\rho(\theta_{3,1})\approx\int_{-2\pi/3T}^{2\pi/3T}\frac{dk}{2\pi}=\frac{1}{3a}\frac{2}{\sqrt{13}} \tag{4.40}$$

in agreement with the Akhmerov et al. result 4.1 using $\theta_{3,1}=13.9^\circ$. The density of zero modes is reduced by a factor of $2/\sqrt{13}\approx.55$ from zigzag.

The real-space zero energy edge mode wavefunctions have the form

$$\alpha_{i,n,m}=e^{iknT}\{g_i(k)\nu_1(k)^m+l_i(k)\nu_2(k)^m\}=e^{iknT}\alpha_{i,m}(k), \tag{4.41}$$

for $i = 1, 2, 3, 4$ where the $g_i(k)$ and $l_i(k)$ are phase factors fully determined in terms of the two normalizable roots $\nu_1(k) and \nu_2(k)$ from the normalization and boundary conditions. We again edge-project the Hubbard interaction. We take the interaction in the site basis $H_U = U \sum_i c^\dagger_{i\uparrow} c_{i\uparrow} c^\dagger_{i\downarrow} c_{i\downarrow}$ and project it into the non-interacting eigenbasis. We neglect bulk-bulk and bulk-edge correlations, sum over the transverse index n, and rename the momenta, obtaining

$$H_U \approx \sum_{kk'q} \Gamma(k, k', q) e^\dagger_\uparrow(k+q) e_\uparrow(k) e^\dagger_\downarrow(k'-q) e_\downarrow(k'), \tag{4.42}$$

valid for $U/t \ll 1$, where the vertex factor $\Gamma(k, k', q)$ is defined in terms of the four wavefunctions $\alpha_{i,m}(k)$ by

$$\Gamma(k, k', q) = LU \sum_{i,m} \alpha_{i,m}(k+q) \alpha^*_{i,m}(k) \alpha_{i,m}(k'-q) \alpha^*_{i,m}(k'). \tag{4.43}$$

Again we define the operators

$$O^\dagger_{i,m}(q) = \sqrt{LU} \sum_k \alpha^*_{i,m}(k+q) \alpha_{i,m}(k) \big[\sum_\sigma e^\dagger_\sigma(k+q) e_\sigma(k) - \delta_{q=0} \big], \tag{4.44}$$

which bring the hamiltonian into positive definite form, exactly as in the $(2, 1)$ case but with one additional term in the sum $i = 1, 2, 3, 4$ over distinct sites in the unit cell at a chosen m:

$$H_U = \sum_{i,m,q} O^\dagger_{i,m}(q) O_{i,m}(q). \tag{4.45}$$

At this point it is again clear from the definition of $O_{i,m}(q)$ that a fully polarized state is annihilated by H_U and is therefore a ground state. We must show these ferromagnetic ground states are the unique ground states.

To this end we again consider the action of $O_{i,m}(q)$ on a ground state $|\psi\rangle$, setting $q \leq 0$ to obtain the condition

$$0 = \sum_{-2\pi/3-qT<kT<2\pi/3} \alpha^*_{i,m}(k+q)\alpha_{i,m}(k)\big[\sum_\sigma e^\dagger_\sigma(k+q)e_\sigma(k) - \delta_{q=0}\big]|\psi\rangle. \tag{4.46}$$

We note $\alpha^*_{i,m}(k+q)\alpha_{i,m}(k) = \alpha^*_{i,m}(-k)\alpha_{i,m}(-k-q)$ and we break the sum into two equal halves $-2\pi/3 - qT < kT \leq -qT/2$ and $-qT/2 \leq kT < 2\pi/3$. We restrict the sum to the upper half of the range and write two terms:

$$\begin{aligned} 0 = \sum_{-qT/2\leq kT<2\pi/3} & \alpha^*_{i,m}(k+q)\alpha_{i,m}(k) \\ & \times \big[\sum_\sigma \{e^\dagger_\sigma(k+q)e_\sigma(k) + e^\dagger_\sigma(-k)e_\sigma(-k-q)\} - 2\delta_{q=0}\big]|\psi\rangle. \end{aligned} \tag{4.47}$$

Again, we would like to argue that the summand vanishes at every k. In the zigzag case we were able to argue this rigorously with the Vandermonde theorem. For the $(2,1)$ case the best we can do is show this invertibility numerically for different choices of L or equivalently different choices of the number of independent momenta.

Fixing the number of unit cells to be L and defining matrix elements and kets via

$$M^i_{m,k}(q) = \alpha^*_{i,m}(k+q)\alpha_{i,m}(k), \tag{4.48}$$

$$|\psi^q_k\rangle = \big[\sum_\sigma \{e^\dagger_\sigma(k+q)e_\sigma(k) + e^\dagger_\sigma(-k)e_\sigma(-k-q)\} - 2\delta_{q=0}\big]|\psi\rangle, \tag{4.49}$$

we can again construct an analogue of the Vandermonde matrix from the zigzag case:

$$\begin{bmatrix} M^i_{0,k_0}(q) & M^i_{0,k_1}(q) & \dots & M^i_{0,k_D}(q) \\ M^i_{1,k_0}(q) & M^i_{1,k_1}(q) & \dots & M^i_{1,k_D}(q) \\ \vdots & \ddots & \ddots & \vdots \\ M^i_{D,k_0}(q) & M^i_{D,k_1}(q) & \dots & M^i_{D,k_D}(q) \end{bmatrix} \begin{bmatrix} |\psi^q_{k_0}\rangle \\ |\psi^q_{k_1}\rangle \\ \vdots \\ |\psi^q_{k_D}\rangle \end{bmatrix} = \begin{bmatrix} 0 \\ 0 \\ \vdots \\ 0 \end{bmatrix}. \tag{4.50}$$

We note this matrix is not of Vandermonde form, but is instead a sum of four Vandermonde matrices. Therefore the approach we used to isolate particular momentum channels for the zigzag ferromagnetism proof does not work here. Instead we have done this numerically for particular cases. We have calculated the determinant of these four matrices (one for each i) to be non-zero at every q for system sizes up to $L = 54$ unit cells, which corresponds to at most a 19×19 matrix. For cases of $L \leq 54$ we obtain our condition

$$\big[\sum_{\sigma}\{e^\dagger_\sigma(k+q)e_\sigma(k) + e^\dagger_\sigma(-k)e_\sigma(-k-q)\} - 2\delta_{q=0}\big]|\psi\rangle = 0, \tag{4.51}$$

from which the proof of edge ferromagnetism on the $(3,1)$ minimal chiral ribbon follows by exact recapitulation of the steps around equations 3.25 to 3.38 in the zigzag proof. We then have a rigorous proof of magnetism for $L \leq 54$. It is plausible that this proof can be done for any L.

Chapter 5

Conclusion

We have reviewed literature relevant to an understanding of confinement-driven magnetism in carbon ribbons with patterned edges. For the simplest case of a zigzag edged ribbon, edge ferromagnetism has been rigorously proven in the small U/t limit by previous authors by projecting a Hubbard interaction onto the localized edge modes and neglecting certain marginal interactions. We have built upon this previous work by numerically demonstrating edge ferromagnetism on minimal chiral ribbons of the $(2,1)$ and $(3,1)$ variety within this edge-projected Hubbard approximation.

Our numerical proof of magnetism within this edge-projected hubbard interaction becomes more difficult for lower chirality ribbons, since we need to concentrate on individual momentum channels in order to rigorously prove magnetism. To isolate individual momentum channels, we must invert a matrix with elements which are products of the zero-energy edge mode wavefunctions. In general, these chiral edge mode wavefunctions cannot be exactly known, and they may also have undetermined coefficients associated with edge-mode degeneracy. These two complications prevent us from inverting these matrices and isolating momentum channels in the general case.

The best we have been able to achieve is show the invertibility of this matrix numerically for many cases, which provides a strong suggestion of edge ferromagnetism on $(2,1)$ and $(3,1)$ chiral ribbons of any length, and a numerical proof of edge ferromagnetism on $(2,1)$ ribbons with $L \leq 192$ and $(3,1)$ ribbons with $L \leq 54$. We expect our methodology is sufficient to numerically demonstrate edge ferromagnetism in any minimal chiral ribbon of a given length supporting non-degenerate edge modes, given we have sufficient computational power to calculate the determinant of the resulting

matrices analogous to those in equation 4.50.

Bibliography

[1] A. R. Akhmerov and C. W. J. Beenakker. Boundary conditions for dirac fermions on a terminated honeycomb lattice. *Phys. Rev. B*, 77:085423, Feb 2008.

[2] L. Brey and H. A. Fertig. Electronic states of graphene nanoribbons studied with the dirac equation. *Phys. Rev. B*, 73:235411, Jun 2006.

[3] A. R. Carvalho, J. H. Warnes, and C. H. Lewenkopf. Edge magnetization and local density of states in chiral graphene nanoribbons. *Phys. Rev. B*, 89:245444, Jun 2014.

[4] A. H. Castro Neto, F. Guinea, N. M. R. Peres, K. S. Novoselov, and A. K. Geim. The electronic properties of graphene. *Rev. Mod. Phys.*, 81:109–162, Jan 2009.

[5] Imre Hagymasi Peter Vanscso-Zoltan Osvath Peter Nemes-Incze Chanyong Hwang Laszlo P. Biro Levente Tapaszto Gabor Zsolt Magda, Xiaozhan Jin. Room-temperature magnetic order on zigzag edges of narrow graphene nanoribbons. *Nature*, 514:608, Sept 2014.

[6] Michael Golor, Thomas C. Lang, and Stefan Wessel. Quantum monte carlo studies of edge magnetism in chiral graphene nanoribbons. *Phys. Rev. B*, 87:155441, Apr 2013.

[7] W. Jaskólski, A. Ayuela, M. Pelc, H. Santos, and L. Chico. Edge states and flat bands in graphene nanoribbons with arbitrary geometries. *Phys. Rev. B*, 83:235424, Jun 2011.

[8] Hamed Karimi and Ian Affleck. Towards a rigorous proof of magnetism on the edges of graphene nanoribbons. *Phys. Rev. B*, 86:115446, Sep 2012.

[9] Kyoko Nakada, Mitsutaka Fujita, Gene Dresselhaus, and Mildred S. Dresselhaus. Edge state in graphene ribbons: Nanometer size effect and edge shape dependence. *Phys. Rev. B*, 54:17954–17961, Dec 1996.

[10] Manuel J. Schmidt, Michael Golor, Thomas C. Lang, and Stefan Wessel. Effective models for strong correlations and edge magnetism in graphene. *Phys. Rev. B*, 87:245431, Jun 2013.

[11] Manuel J. Schmidt and Daniel Loss. Tunable edge magnetism at graphene/graphane interfaces. *Phys. Rev. B*, 82:085422, Aug 2010.

[12] Young-Woo Son, Marvin L. Cohen, and Steven G. Louie. Energy gaps in graphene nanoribbons. *Phys. Rev. Lett.*, 97:216803, Nov 2006.

[13] Liying; Yazyev Oleg V.; Chen Yen-Chia; Feng Juanjuan; Zhang-Xiaowei; Capaz Rodrigo B.; Tour James M.; Zettl Alex; Louie Steven G.; Dai Hongjie; Tao, Chenggang; Jiao and Michael F. Crommie. Spatially resolving edge states of chiral graphene nanoribbons. *Nat Phys*, 7:616–620, Aug 2011.

[14] Katsunori Wakabayashi, Yositake Takane, Masayuki Yamamoto, and Manfred Sigrist. Electronic transport properties of graphene nanoribbons. *New Journal of Physics*, 11(9):095016, 2009.

[15] T. O. Wehling, E. Şaşıoğlu, C. Friedrich, A. I. Lichtenstein, M. I. Katsnelson, and S. Blügel. Strength of effective coulomb interactions in graphene and graphite. *Phys. Rev. Lett.*, 106:236805, Jun 2011.

[16] Oleg V. Yazyev, Rodrigo B. Capaz, and Steven G. Louie. Theory of magnetic edge states in chiral graphene nanoribbons. *Phys. Rev. B*, 84:115406, Sep 2011.

The Vandermonde Argument for Zigzag

Here we will show equation 3.24 holds given equation 3.23.

We begin from equation 3.23, and we set $q \leq 0$ so the range of k in the sum can be written $2\pi/3 - qa < ka < 4\pi/3$:

$$0 = \sum_{2\pi/3-qa<ka<4\pi/3} \alpha_m^*(k)\alpha_m(k+q) \times \big[\sum_\sigma e_\sigma^\dagger(k+q)e_\sigma(k) - \delta_{q=0}\big]|\psi\rangle. \quad (1)$$

Now we perform a series of manipulations on this equation. First, we shift all ka by π so the range of allowed momenta becomes $-\pi/3 - qa < ka < \pi/3$– this is just for convenience. We have

$$\alpha_m^*(k)\alpha_m(k+q) \propto \sin\{ka/2\}\sin\{(k+q)a/2\} = \frac{1}{2}\{\cos(qa/2) - \cos(ka+qa/2)\} \quad (2)$$

by double-angle formulas. We can see two values of k in the range $-\pi/3 - qa < ka < \pi/3$ will give equal values of $\alpha_m^*(k)\alpha_m(k+q)$. We determine these values k, k' by requiring

$$\cos(ka + qa/2) = \cos(k'a + qa/2) \quad (3)$$

which has the solution

$$k' = -k - q. \tag{4}$$

We would like to manipulate equation 1 into a form whereby each term in the sum over k must vanish independently. It is convenient to break the sum into two equal halves $-\pi/3 - qa < ka \leq -qa/2$ and $-qa/2 \leq ka < \pi/3$. We see that $-qa/2 \leq ka < \pi/3$ places $k' = -k - q$ into the range $-\pi/3 - qa < k'a \leq -qa/2$. This allows us to restrict the sum in equation 1 to the upper half at the expense of writing two terms:

$$\begin{aligned} 0 = \sum_{-qa/2 \leq ka < \pi/3} & \alpha_m^*(k)\alpha_m(k+q) \\ & \times \big[\sum_\sigma \{e_\sigma^\dagger(k+q)e_\sigma(k) + e_\sigma^\dagger(-k)e_\sigma(-k-q)\} - 2\delta_{q=0} \big] |\psi\rangle. \end{aligned} \tag{5}$$

In writing this, we have used the property $\alpha_m^*(k)\alpha_m(k+q) = \alpha_m^*(-k-q)\alpha_m(-k)$ of the wavefunctions which can be seen from their definition 3.16.

Now we will show that each term in this sum vanishes independently. Our argument hinges upon the Vandermonde theorem concerning the determinant of a particular (said to be of Vandermonde form) square matrix:

$$\begin{vmatrix} x_0^0 & x_1^0 & x_2^0 & \dots & x_n^0 \\ x_0^1 & x_1^1 & x_2^1 & \dots & x_n^1 \\ \vdots & \dots & \ddots & \dots & \vdots \\ x_0^n & x_1^n & x_2^n & \dots & x_n^n \end{vmatrix} \propto \prod_{i<j} (x_i - x_j). \tag{6}$$

Notice if every x_i is distinct, the Vandermonde determinant is necessarily non-vanishing, meaning the matrix is invertible. Now let us use the explicit form of the wavefunctions $\alpha_m(k)$ from equation 3.7, remembering we have shifted ka by π, and denoting

$$\begin{aligned} |\psi_k^q\rangle = e^{iqam/2} & \alpha_0^*(k)\alpha_0(k+q) \\ & \times \big[\sum_\sigma \{e_\sigma^\dagger(k+q)e_\sigma(k) + e_\sigma^\dagger(-k)e_\sigma(-k-q)\} - 2\delta_{q=0} \big] |\psi\rangle \end{aligned} \tag{7}$$

and

$$M_k(q) = 4\sin\big[\frac{ka}{2}\big]\sin\big[\frac{(k+q)a}{2}\big]. \tag{8}$$

Equation 5 takes the simple-looking form:

$$0 = \sum_{-qa/2 \le ka < \pi/3} M_k(q)^m |\psi_k^q\rangle. \tag{9}$$

Consider a zigzag ribbon of finite length L. There are at most $L/3+1$ allowed momenta k in the range $-\pi/3 - qa < ka < \pi/3$, and at most $L/6+1$ independent momenta to sum over in 9. Denote the set of momenta in this range k_0, k_1, ...,k_D.

Since equation 9 holds for every m, the index describing distance away from the ribbon edge, which ranges from 0 to ∞ in integer steps, we can write down the equation for the first $D+1$ values of m and form a $(D+1)\times(D+1)$ square matrix:

$$\begin{bmatrix} M_{k_0}(q)^0 & M_{k_1}(q)^0 & \dots & M_{k_D}(q)^0 \\ M_{k_0}(q)^1 & M_{k_1}(q)^1 & \dots & M_{k_D}(q)^1 \\ \vdots & \ddots & \ddots & \vdots \\ M_{k_0}(q)^D & M_{k_1}(q)^D & \dots & M_{k_D}(q)^D \end{bmatrix} \begin{bmatrix} |\psi_{k_0}^q\rangle \\ |\psi_{k_1}^q\rangle \\ \vdots \\ |\psi_{k_D}^q\rangle \end{bmatrix} = \begin{bmatrix} 0 \\ 0 \\ \vdots \\ 0 \end{bmatrix}. \tag{10}$$

We note this matrix is of Vandermonde form. We have purposefully manipulated the range of k in the sum in equation 9 to ensure $M_k(q)$ is single-valued and non-zero with k on this range for any $q \le 0$. Therefore, the Vandermonde determinant is non-zero, and we can invert the Vandermonde matrix to obtain

$$0 = \big[\sum_\sigma \{e_\sigma^\dagger(k+q)e_\sigma(k) + e_\sigma^\dagger(-k)e_\sigma(-k-q)\} - 2\delta_{q=0}\big]|\psi\rangle \tag{11}$$

as claimed in equation 3.24.